HREM Study of Epitaxially Stabilized Hexagonal Rare Earth Manganites

I. E. Graboy,[†] A. A. Bosak,*[,†,‡] O. Yu. Gorbenko,[†] A. R. Kaul,[†] C. Dubourdieu,[‡] J.-P. Sénateur,[‡] V. L. Svetchnikov,[§] and H. W. Zandbergen[§]

Department of Chemistry, Moscow State University, 119899 Moscow, Russia, LMGP, UMR 5628 CNRS, ENSPG, BP 46, 38402 St. Martin d'Hères, France, and National Centre for HREM, Laboratory of Materials Science, Delft University of Technology, Rotterdamseweg 137, 2628 AL Delft, The Netherlands

Received September 23, 2002. Revised Manuscript Received February 25, 2003

The formation of the high-temperature hexagonal modification of $DyMnO_3$ and nonexisting as bulk hexagonal $EuMnO_3$, $GdMnO_3$, and $SmMnO_3$ was observed on $ZrO_2(Y_2O_3)$ (111) substrates at 900 °C due to epitaxial stabilization. HREM study reveals epitaxial growth of the hexagonal film of limited thickness depending on the nature of the rare earth cation. For thickness exceeding critical, the oriented stable perovskite form grows semicoherently on the hexagonal phase. The interface of two polymorphs is not abrupt and involves the formation of the transition zone with the characteristic pyramid-like shapes on the top of the hexagonal layer. The typical structural defects in the hexagonal $RMnO_3$ films are described.

1. Introduction

$RMnO_3$ compounds, where R is a trivalent rare earth cation, possess perovskite structure for rare earth cations with larger ionic radius. Stable hexagonal $LuMnO_3$-type structure (space group $P6_3cm$) has been found for $RMnO_3$ compounds in the case of R with small ionic radius (Ho−Lu, Y, Sc). This structure can be described as dense oxygen-ion packing (ABCACB) with Mn^{3+} ions having coordination number CN = 5 (5-fold trigonal bipyramidal coordination) and R^{3+} with CN = 7 (7-fold monocapped octahedral coordination)[1] (see Figure 1a). $YMnO_3$, which belongs to this structural type, is considered to be potential ferroelectric material for electronic applications.[2]

A perovskite phase with space group *Pnma* (see Figure 1b) can be obtained for R = Y, Ho−Lu instead of hexagonal $RMnO_3$ by high-pressure synthesis,[3] by "soft chemistry" synthesis,[4] or by the epitaxy on perovskite substrates.[5] The requirement of high pressure can be easily understood, taking into account the significant decrease of the unit cell volume (8−9%) from hexagonal to perovskite structure,[1] as shown in Figure 2, where the normalized unit cell volume is traced vs tolerance factor *t*. When considering the RBO_3 series of various 3d elements, the stable hexagonal structure is only observed for $RMnO_3$ compounds, but metastable hexagonal phases are known for some gallates and aluminates. It is interesting to note that both the perovskite and the hexagonal series correspond to nearly linear plots in Figure 2. As both series are observed in the same tolerance factor *t* range, it seems that there is no geometrical limitation on hexagonal phase formation. So the criteria of a polymorph formation should be of an energetic nature correlating with an energy difference between an octahedron in perovskite and a less symmetrical polyhedron of 3d ions—trigonal bipyramid—in hexagonal phases.[6]

For $DyMnO_3$ the free energies of two polymorphs are very close: stable modification is perovskite, and the hexagonal phase was obtained by quenching from high temperature (≥1600 °C).[4] But for larger rare earth ions such as Gd^{3+} direct extrapolation of transition temperature gives too high phase transition temperature (about 2800 °C, which is well above the melting point of manganites).

In our previous work[7] we have demonstrated that a suitable method for synthesis of metastable hexagonal manganites is epitaxial stabilization. The calculations made using available data for stable hexagonal phases show that $ZrO_2(Y_2O_3)$ (111) cubic substrate (the atomic ratio $Y/(Y + Zr) = 0.15$) has in-plane lattice parameters closest to those of hypothetical hexagonal phases ($R > R_{Dy}$) (Figure 3) and excellent coincidence of oxygen crystallographic positions at the interface. Thin epitaxial films of hexagonal $RMnO_3$, which are unstable in bulk under usual conditions, were deposited by the MOCVD technique on appropriate (111) $ZrO_2(Y_2O_3)$

* Corresponding author: Tel.: +007 (095) 9391492. Fax: +007 (095) 9391492. E-mail: bossak@inorg.chem.msu.ru.
† Moscow State University.
‡ CNRS.
§ Delft University of Technology.

(1) Yakel, H. L.; Koehler, W. C.; Bertaud, E. F.; Forrat, E. F. *Acta Crystallogr.* **1963**, *16*, 957.
(2) Fujimura, N.; Ishida, T.; Yoshimura, T.; Ito, T. *Appl. Phys. Lett.* **1996**, *69*, 1011.
(3) Waintal, A.; Chenavas, J. *Mater. Res. Bull.* **1967**, *2*, 819.
(4) Szabo, G. Thèse, University of Lyon, Lyon, France, 1969.
(5) Bosak, A. A.; Kamenev, A. A.; Graboy, I. E.; Antonov, S. V.; Gorbenko, O. Yu.; Kaul, A. R.; Dubourdieu, C.; Senateur, J.-P.; Svechnikov, V. L.; Zandbergen, H. W.; Holländer, B. *Thin Solid Films* **2001**, *400*, 149.
(6) Reznitskii, L. A. *Neorg. Mater.* (in Russian) **1984**, *20*, 743.
(7) Bosak, A. A.; Dubourdieu, C.; Sénateur, J.-P.; Gorbenko, O. Yu.; Kaul, A. R. *J. Mater. Chem.* **2002**, *12*, 800.

10.1021/cm021315b CCC: $25.00
Published on Web 05/31/2003

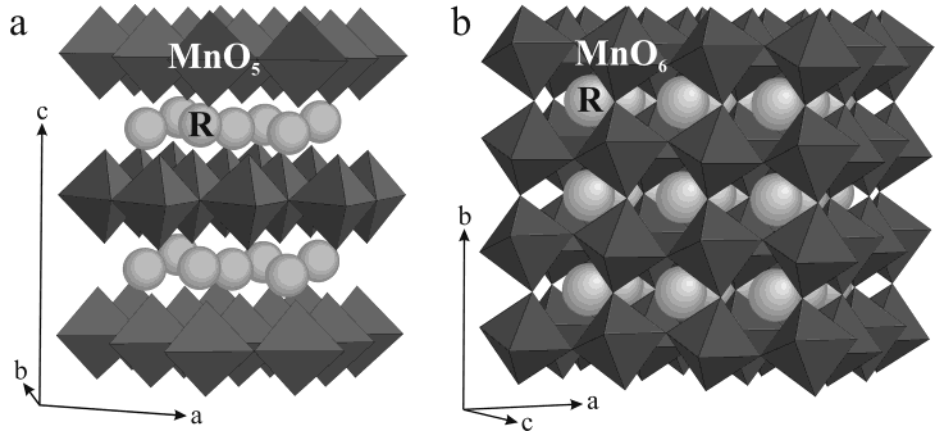

Figure 1. Crystal structures of $LuMnO_3$-type hexagonal phases (a) and perovskite orthorhombic phases (b).

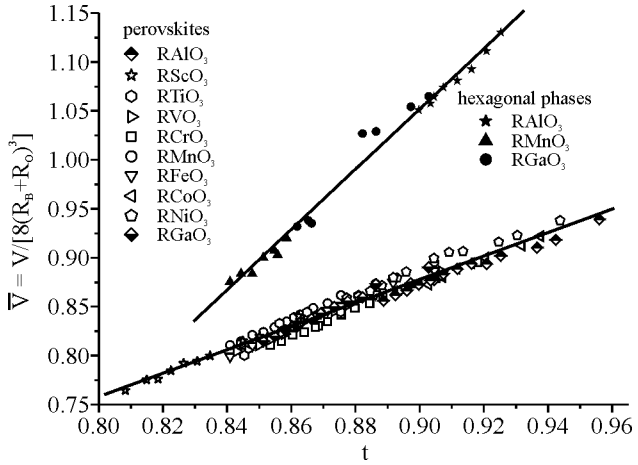

Figure 2. Dependence of the normalized unit cell volume per formula unit vs tolerance factor (JCPDS data and [refs 4, 8, and 9]).

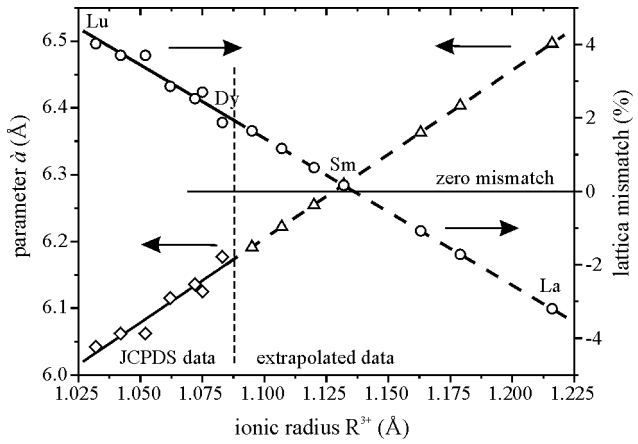

Figure 3. Calculated lattice mismatch with $ZrO_2(Y_2O_3)$ (111) substrate; mismatch is given as $M = 1 - (\bar{a}/a_S)$.

substrates and studied in detail by X-ray diffraction (XRD). Epitaxial relations were established as follows:

$$(001)_{hex.}\ RMnO_3 \,//\, (111)\ ZrO_2(Y_2O_3);$$
$$\langle 1\bar{1}0\rangle_{hex.}\ RMnO_3 \,//\, \langle 1\bar{1}0\rangle\ ZrO_2(Y_2O_3)$$

The hexagonal phase is stabilized by the energy gain due to coherent interface formation as in the case of other systems studied by our scientific group: $BaCu_3O_4$,[10] $RNiO_3$,[11] $NdMn_7O_{12}$,[12] and $RCoO_3$.

Table 1. Atomic Coordinates Used in ED and HREM Modeling for $DyMnO_3$ and $ZrO_2(Y_2O_3)$

$DyMnO_3$	$P6_3cm$			$ZrO_2Y_2O_3$)	$Pm3m$		
Lu(1)	0	0	0.2705	Zr(Y)	0	0	0
Lu(2)	$^1/_3$	$^2/_3$	0.2266	O	$^1/_4$	$^1/_4$	$^1/_4$
Mn	0.3212	0	0				
O(1)	0.3071	0	0.1699				
O(2)	0.6328	0	0.3397				
O(3)	0	0	0.4836				
O(4)	$^1/_3$	$^2/_3$	0.0189				

Here, we present the results of the HREM study of the epitaxially stabilized hexagonal $RMnO_3$ films and compare them to the earlier results obtained by XRD.

2. Experiment

The deposition of films with approximate thickness 600−700 Å was performed on $ZrO_2(Y_2O_3)$ (111) using a liquid injection MOCVD device[13] as described in ref 7. The films were characterized by high-resolution electron microscopy (HREM). Cross sections of ion-milled film samples were studied using microscope Philips CM30UT with a field emission gun operated at 300 kV. Electron diffraction patterns were recorded with a 1024 × 1024 pixel Photometrix CCD camera with a dynamic range of 12 bits. Electron diffraction (ED) was performed with spot sizes of about 10 nm, using a 15-μm condenser lens aperture. Exposure times ranged from 0.5 to 2 s. ED and HREM simulation was performed by MacTempas PPC software using the atomic coordinates for $LuMnO_3$ together with determined here unit cell parameters (atomic coordinates used are summarized in Table 1).

3. Results and Discussion

The epitaxy is evident from HREM observations for hexagonal $DyMnO_3$, $GdMnO_3$, and $EuMnO_3$ films. HREM images and ED patterns (Figure 4) were obtained from a cross section along the $[1\bar{1}0]$ zone of the $ZrO_2(Y_2O_3)$ substrate. Structure type and block orienta-

(8) Geller, S.; Jeffries, J. B.; Curlander, P. J. *Acta Crystallogr.* **1975**, *B31*, 2770.
(9) Sallavuard, G.; Szabo, G.; Pris, R.-A. *C. R. Acad. Sci. Paris* **1969**, *268*, 1050.
(10) Samoylenkov, S. V.; Gorbenko, O. Yu.; Graboy, I. E.; Kaul, A. R.; Zandbergen, H. W.; Connolly, E. *Chem. Mater.* **1999**, *11*, 2417.
(11) Novojilov, M. A.; Gorbenko, O. Yu.; Graboy, I. E.; Kaul, A. R.; Zandbergen, H. W. *Appl. Phys. Lett.* **2000**, *76*, 2041.
(12) Bosak, A. A.; Gorbenko, O. Yu.; Kaul, A. R.; Graboy, I. E.; Dubourdieu, C.; Senateur, J. P.; Zandbergen, H. W. *J. Magn. Magn. Mater.* **2000**, *211*, 61.
(13) Sénateur, J. P.; Dubourdieu, C.; Weiss, F.; Rosina, M.; Abrutis, A. *Adv. Mater. Opt. Electron.* **2000**, *10*, 155.

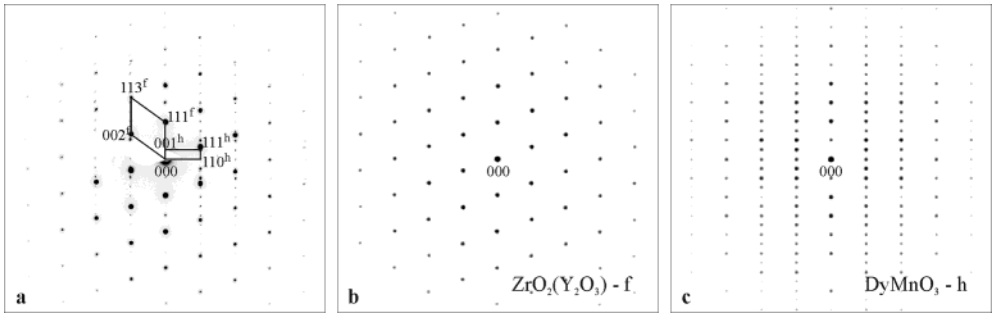

Figure 4. $(1\bar{1}0)$ zone diffraction pattern (a); ED model (b) and (c). Superscript "f" corresponds to the fluorite substrate and "h" corresponds to the hexagonal phase.

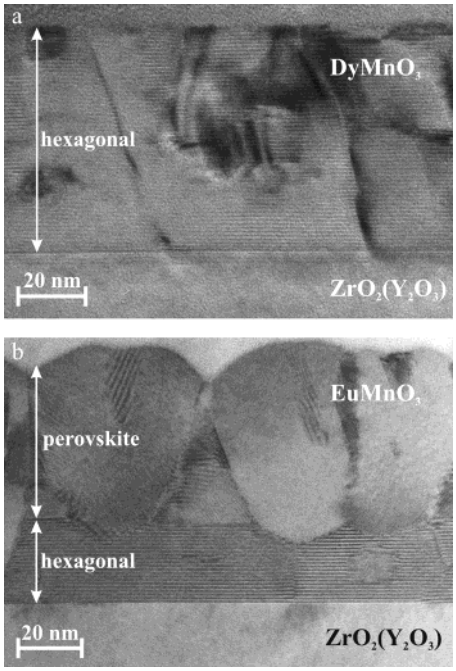

Figure 5. $(1\bar{1}0)$ zone general view of hexagonal films on ZrO_2-(Y_2O_3) (111): (a) $DyMnO_3$; (b) $EuMnO_3$

tions are consistent with $LuMnO_3$-type hexagonal structure. While no significant quantities of secondary orientations or secondary phases are visible on low-resolution images, block structure is clearly seen (Figure 5a). These blocks can be usually considered as obtained by the rotation by $\pi/3$ and shift by $\sim c/6$ (or only shift by $\sim c/3$).

No regular misfit dislocations are found (Figure 6), indicating that the films are strained in accordance with the XRD data[7] (the expected density for unstrained film is $10-12\ \underline{\mu}m^{-1}$). The simulated image of hexagonal phase ($[1\bar{1}0]$ zone) fits the experimentally observed image well. Domain boundaries are usually extended antiphase boundaries generated by substrate steps (one monolayer step giving an antiphase boundary is shown in Figure 7a) and they can also be annihilated on stacking faults (Figure 7b). The idealized model of an antiphase boundary is given in Figure 7d (related to the stacking sequence from the high-resolution image in Figure 7c).

In addition, we have found singular inclusions of particles which are identical to the hexagonal matrix but rotated around the $\langle 1\bar{1}0\rangle$ direction (Figure 8) so the orientation relations become

$$(111)\ RMnO_3^{incl.} \,//\, (001)\ RMnO_3^{matrix};$$
$$\langle 1\bar{1}0\rangle\ RMnO_3^{incl.} \,//\, \langle 1\bar{1}0\rangle\ RMnO_3^{matrix}$$

The appearance of secondary orientation of hexagonal $DyMnO_3$ instead of perovskite can be explained by the very proximity of polymorphs free energies so even the semicoherent interface (defined after ref 14) is sufficient to provide epitaxial stabilization.

Following generalized thermodynamic estimation,[10] when the energy gap between equilibrium in the bulk state and nonequilibrium in the bulk state does not exceed 10−15 kJ/mol, the latter can be stabilized by the free energy gained from diminishing the surface energy term due to coherent interface formation. (The extended review on the epitaxial stabilization of oxide materials together with the quantitative estimations is recently published.[15])

For our systems the stabilization energy can be estimated using the linear extrapolation of bulk $RMnO_3$ formation energy dependencies vs ionic radius (Figure 9). It attains the maximum value of 7−10 kJ/mol for Eu−Sm. It should be noted that the extension of the region of epitaxial stabilization in the energy scale is nearly the same for the hexagonal phases as found for

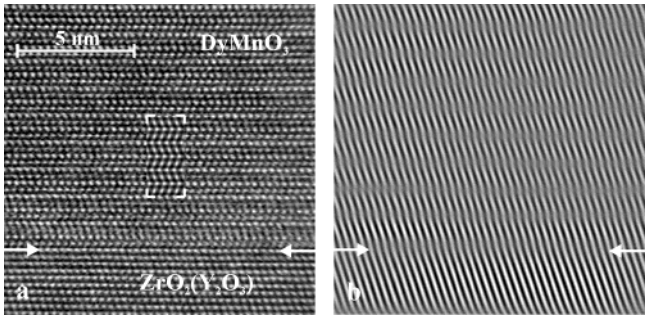

Figure 6. $[1\bar{1}0]$ zone high-resolution image of $DyMnO_3/ZrO_2(Y_2O_3)$ (a) and Fourier-filtered image (b). The inset demonstrates the simulation of a HREM image with MacTempas PPC software.

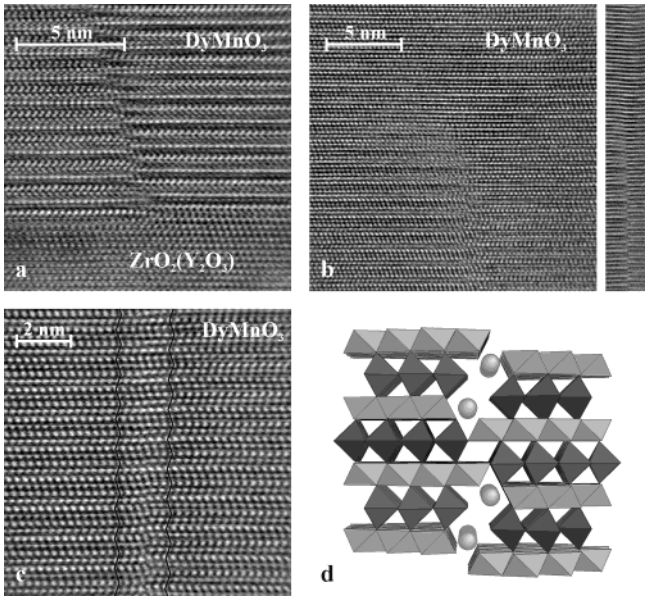

Figure 7. Antiphase boundaries: (a) generation by substrate step; (b) annihilation on stacking fault; (c) high-resolution image; and (d) idealized model.

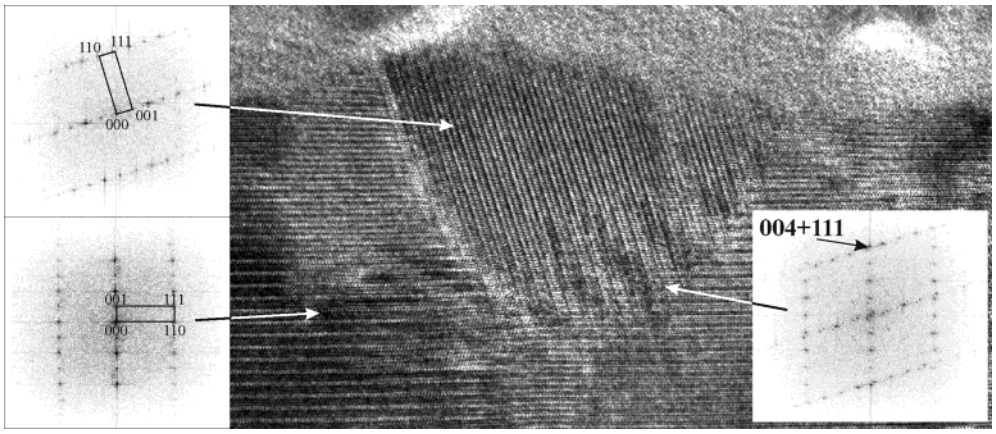

Figure 8. HREM image of area containing secondary orientation. Fourier transforms of selected regions are added for clarity.

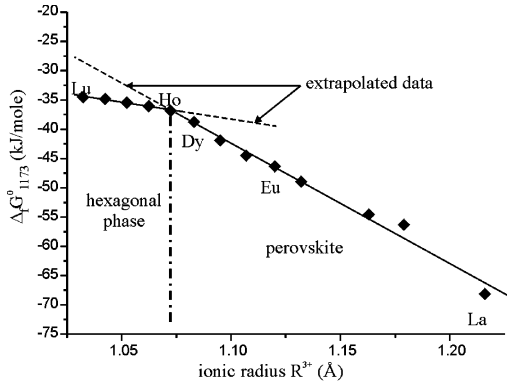

Figure 9. Free energy of $RMnO_3$ formation from R_2O_3 and Mn_2O_3 at 900 °C (calculated using oxygen dissociation pressure data[16]).

perovskite manganites.[5] As the contribution of the surface energy is inversely dependent on the thickness, the stabilizing effect can only be observed for the films of limited thickness.[10] $GdMnO_3$ thin films do not crystallize completely in a pure hexagonal phase, and the upper layer is of perovskite structure. This tendency is even more pronounced for $EuMnO_3$ (Figure 5b). Orthorhombic perovskite grows as follows (Figure 10a,b):

$$(001)\ RMnO_3^{orth.} \parallel (001)\ RMnO_3^{hex.};$$
$$\langle 010\rangle\ RMnO_3^{orth.} \parallel \langle 1\bar{1}0\rangle\ RMnO_3^{hex.}$$

$$(100)\ RMnO_3^{orth.} \parallel (001)\ RMnO_3^{hex.};$$
$$\langle 010\rangle\ RMnO_3^{orth.} \parallel \langle 1\bar{1}0\rangle\ RMnO_3^{hex.}$$

The choice of this main orientation is probably due to a good lattice match in the $\langle 1\bar{1}0\rangle\ RMnO_3^{hex.}$ direction (mismatch 2−3%).

Secondary orientation appears as follows (Figure 10c):

$$(201)\ RMnO_3^{orth.} \parallel (001)\ RMnO_3^{hex.};$$
$$\langle 10\bar{2}\rangle\ RMnO_3^{orth.} \parallel \langle 110\rangle\ RMnO_3^{hex.}$$

$$(102)\ RMnO_3^{orth.} \parallel (001)\ RMnO_3^{hex.};$$
$$\langle 20\bar{1}\rangle\ RMnO_3^{orth.} \parallel \langle 110\rangle\ RMnO_3^{hex.}$$

(14) Sutton, A. P.; Balluffi, R. W. *Interfaces in Crystalline Materials*; Clarendon Press: Oxford, 1995.
(15) Gorbenko, O.; Kaul, A. R.; Graboy, I. E.; Samoilenkov, S. V. *Chem. Mater.* **2002**, *14*, 4026.

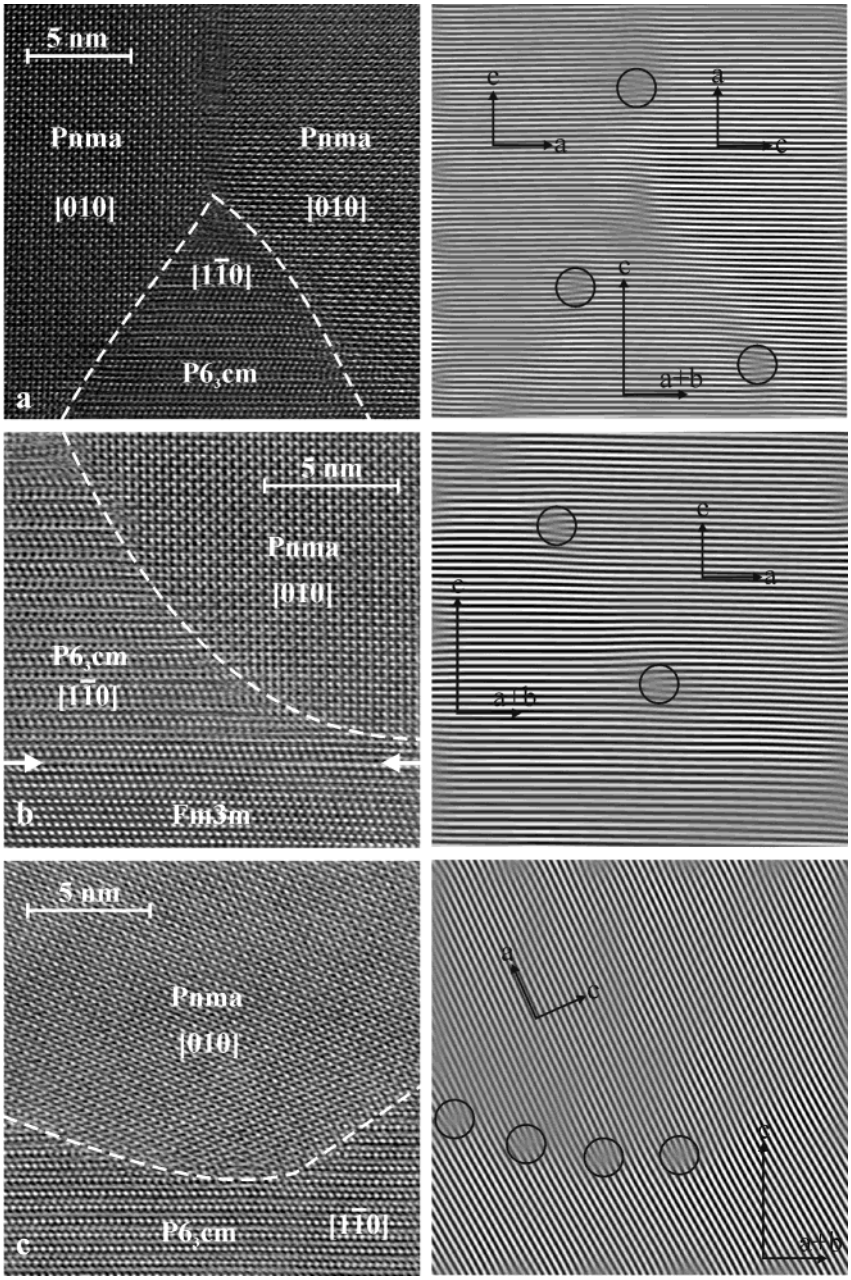

Figure 10. HREM image of the transition region in $EuMnO_3$. The dashed lines denote the boundary of the hexagonal and perovskite phases. Images on the right side are Fourier-filtered images (misfit dislocations and crystallographic orientation are shown as guides for the eye).

As the crystal structures of perovskite and hexagonal phases are completely different (Figure 1), the perovskite cannot form due to a phase transition related to epitaxial strain, but only by nucleation on the top of the hexagonal layer. This critical thickness of the hexagonal layer decreases with the increase of the bulk free energy gap between perovskite and hexagonal phase.

The hexagonal phase switches to perovskite in the transition zone of the film where the phases coexist, being separated with semicoherent interfaces. The interface is rather flattened on the hexagonal side of the zone and much steeper on the perovskite side of the transition layer, resulting in the characteristic pyramid-like morphology (Figure 10). This behavior can be explained using the model of Little and Zangwill considering different contributions to the free energy of the thin film system.[17] After the second phase nucleation on the flat surface of the hexagonal layer, the homogeneous lattice strain contribution to energy balance (which destabilizes the hexagonal phase) is diminished sharply, so further switching is retarded. The linear thickness dependence of the energy terms driving the transition (difference in the free energy of the competing phases, interface energy, and interphase strain energy) results in the pyramid-like shape. These features are all clearly demonstrated in Figure 10. Similar evolution with the growth of the film thickness was observed earlier in the epitaxially stabilized $RNiO_3$ films.[11] Probably such a transition zone is a common feature of epitaxial stabilization with thermodynamic control.

(16) Atsumi, T.; Oghushi, T.; Kamegashira, N. *J. Alloys Compd.* **1996**, *238*, 35.
(17) Little, S.; Zangwill, A. *Phys. Rev. B* **1994**, *49*, 16659.

4. Conclusion

Thus, we have confirmed the epitaxial growth of hexagonal $RMnO_3$ (R = Dy, Gd, Eu, Sm) by HREM. For Gd, Eu, and Sm these phases apparently can not exist as bulk. These phases can be formed with the hexagonal structure (instead of the stable perovskite one) because of epitaxial stabilization of the phases on the oxide substrate with fluorite structure of the proper orientation (111). The stabilization effect is valid only for restricted thickness of the film. At higher thickness the gradual switching to the perovskite phase with the formation of the characteristic pyramid-like morphology can be explained by the explicit consideration of the energy balance.

Acknowledgment. This work was partly supported by RFBR (No. 02-03-33258), VW Stiftung (I/77821), NWO Program (No. 047-008-017), INTAS (No. 01-2008), and CRDF (No. RP2-2355-MO02) projects.

CM021315B